Materials Characterization 119 (2016) 47–54

Contents lists available at ScienceDirect

Materials Characterization

journal homepage: www.elsevier.com/locate/matchar

Enhanced fracture toughness in an annealed Al-Cu-Mg alloy by increasing Goss/Brass texture ratio

Qi Zhao, Zhiyi Liu *, Tiantian Huang, Peng Xia, Fudong Li

[a] Key Laboratory of Nonferrous Metal Materials Science and Engineering, Ministry of Education, Central South University, Changsha 410083, PR China
[b] School of Material Science and Engineering, Central South University, Changsha 410083, PR China

ARTICLE INFO

Article history:
Received 4 May 2016
Received in revised form 15 July 2016
Accepted 17 July 2016
Available online 19 July 2016

Keywords:
Al-Cu-Mg alloy
Texture
EBSD
Fracture toughness

ABSTRACT

The effect of grain orientation on fracture toughness of an annealed Al-Cu-Mg alloy has been investigated by using XRD, SEM, OM and EBSD in the present work. A new method has been presented to accurately evaluate the twist and tilt angle of grain boundaries. EBSD detection results indicate Goss-grains in the annealed Al-Cu-Mg alloy, having a great twist angle or tilt angle component boundary with the neighboring grains, are still able to facilitate crack deflection under the condition of uniaxial tensile stress creating no crack closure, as compared with cyclic loading condition with crack closure in fatigue testing. Goss-grains, thereby effectively retard fracture crack propagation. In contrast, the fast-propagating crack is easy to penetrate through Brass-, S- and Copper-grains. Apparently, the high Goss/Brass volume fraction ratio is responsible for the enhanced fracture toughness in the Al-Cu-Mg alloy plate annealed at 385 °C for 4 h.

1. Introduction

Studies of grain orientation effect on final mechanical properties of metal materials have attracted more and more attention in recent years. It has been reported that textures have a great effect on tensile property anisotropy of aluminum alloys [1–5]. Grain orientation effect on cyclic deformation behavior of copper bicrystals, columnar crystals and tricrystals, was investigated by Wang et al. [4], and their results found that large angle grain boundaries could obstruct the passage of persistent slip bands and subsequently served as the nucleation sites for fatigue cracking. Chen et al. [5] suggested that the strength of the X2095 alloy in the transverse direction was greater than that in the longitudinal direction and that the specimens in the longitudinal loading direction (L-T orientation) exhibited higher fatigue thresholds and lower crack propagation rates than that in the transverse loading direction (T-L orientation) because of the existence of texture consisting of Brass, Copper and S components with Brass being the dominant component. Zhai et al. [6] proposed a crystallographic model for short fatigue crack propagating through grain boundaries, and suggested that the twist and tilt angles of the crack-plane deflection at a grain boundary were the key factors that control the process of crack retardation and deflection at the grain boundary in planar slip alloys. In 2005, Zhai et al. [7] found a large twist angle of the crack plane deflection at the grain boundary gave rise to a higher resistance to crack growth across the grain boundary, while a small twist angle represented a smaller resistance. Their result also suggested that Goss-grains were more resistant to crack growth across their boundaries than Brass-grains in Al-Li and Al-Cu alloys. Liu et al. [8] further confirmed that Goss-grains had a great twist component boundary or tilt angle component boundary with the neighboring grains in an AA2524 T3 alloy, thereby retarding fatigue crack propagation, but Brass-grains exhibited a small resistance to fatigue crack propagation. The recent studies also suggested fatigue performance could benefit from decreasing the intensity of Brass texture [9].

However, all previous work [4–9] stated above, referred to fatigue behavior or performance. Generally in fatigue testing, a cyclic loading is employed, which normally is far below yield strength. Therefore, a crack closure effect is created during fatigue crack propagation. Nevertheless, in fracture toughness testing a uniaxial tensile stress, normally close to yield strength, is employed. Under this stress condition, no crack closure effect is created during crack propagation. Furthermore, crack propagation rate in fracture toughness testing is more rapid than that in fatigue testing. The crack propagation behavior in fracture toughness testing is distinctly different from fatigue crack propagation. Although the effect of Goss- and Brass-grains on fatigue behavior has been well investigated [7–9], no work has been done concerning the effect of Goss- and Brass-grains on fracture toughness. What's more, it is still unknown whether Goss-grains, other than Brass-grains, could also retard crack propagation during fracture toughness testing as it acts in fatigue testing. In addition, it remains unknown whether other grains like S- and Copper-grains have similar mechanism with Goss- or Brass-grains and effect on fracture toughness. A major goal of this report

* Corresponding author at: Key Laboratory of Nonferrous Metal Materials Science and Engineering, Ministry of Education, Central South University, Changsha 410083, PR China.
E-mail address: liuzhiyi335@163.com (Z. Liu).

http://dx.doi.org/10.1016/j.matchar.2016.07.015
1044-5803/

is to investigate the effect of Goss-, Brass-, S- and Copper-grains on fracture toughness of annealed Al-Cu-Mg alloy plates. We also have proposed a new method to accurately evaluate the twist and tilt angle of grain boundaries.

2. Experiments

The material used in this investigation was an Al-Cu-Mg alloy ingot which had a composition (wt%) of 0.05% Si, 0.11% Fe, 0.5% Mn, 1.6% Mg, 4.0% Cu with balance Al. After homogenized at 495 °C for 48 h, the ingots were hot rolled to 88% reduction followed by an isothermal anneal at five different temperatures (300, 320, 340, 360 and 385 °C) for 4 h. Hot rolling began at a temperature of 430 °C and accomplished at 310 °C. Texture measurement using X-ray diffraction (XRD) was performed at the center position of the rolled and annealed material. The (111), (200), and (220) pole figures were measured up to a maximum tilt angle of 75° by the Schulz back reflection method using CuKα radiation. The orientation distribution functions (ODFs) were calculated from these incomplete pole figures and presented as plots of constant φ2 sections with isointensity contours in Euler space defined by the Euler angles φ1, Φ, and φ2. Volume fractions of measured ideal orientations were calculated by integration within 15° of the ideal orientation peaks [10,11].

The tensile test of alloy plates was performed on an Instron testing machine with a cross-head speed of 2 mm/min. The loading direction upon test was along the transverse direction (T); the corresponding value of tensile strength (σ_b), yield strength ($\sigma_{0.2}$) and elongation were obtained. The values of tensile tests were the average value of five measurements. The plane-strain fracture toughness tests were performed on compact-tension specimens according to the ASTM E399 standard. The tests were conducted on an MTS machine at room temperature and laboratory air environment. Compact-tension specimens were prepared from the plates in the L-T orientation with a size (in mm) of 45.6 × 38 × 6 (L × W × B), where L-T signified that the loading direction was along the longitudinal/rolling direction (L) and the direction of the crack growth was oriented along the transverse direction (T). The values of fracture toughness were obtained by the average value of five measurements. Fracture surfaces of failed specimens were examined in a scanning electron microscope (SEM) to determine the predominant macroscopic fracture mode and to characterize the fine-scale topography and features on the fracture surface. Optical metallography (OM) was used to examine the micro-structures. Surfaces were prepared by electropolishing and then anodising with 16.8 g/L fluoroboric acid at 20 V for 60–120 s. Grain size was analyzed using digital image analysis attached to optical microscope. To detect the relationship between fracture crack path, crack deflection and grain orientation or micro-texture in fracture fibrous region, the plates were unloaded when fracture cracks propagated to 20 mm in length. The monitoring of fracture crack lengths was carried out by using a microscopy with a magnification of 100×, measured with solution of 0.01 mm. Electron backscattering diffraction (EBSD) plates were prepared by conventional mechanical grinding and subsequent electropolishing. The electro-polishing was carried out at 18–22 V for 8–15 s by a direct current (DC) stabilized power supply, and the mixed solution for electropolishing was composed of 10% perchloric acid and 90% ethanol. EBSD mapping on rolled plane of specimens were obtained by automatic scanning with a step (pixel) size of 0.2 μm, and the mapping was carried out using a Sirion 200 field emission gun scanning electron microscope with an accelerating voltage of 20 kV.

3. Results

The results of tensile test present that the tensile strength (σ_b) and yield strength ($\sigma_{0.2}$) of hot rolled alloy plate are higher than that of annealed plates, and the elongation of hot rolled plate is lower than that of annealed plates, as shown in Fig. 1. There is a minor change in the tensile strength of annealed plates as the annealing temperature increasing from 300 °C to 340 °C, and then the tensile strength starts to increases gradually with the temperature further increasing from 340 °C to 385 °C. The maximum tensile strength (about 301.1 Mpa) of annealed plate is obtained when the annealing temperature is at 385 °C. The yield strength of annealed plate starts to decreases gradually as the temperature increasing from 300 °C to 360 °C, reaching a bottom in 360 °C, and then moderately increases to 193.9 Mpa as the temperature reaching 385 °C. In contrast, the elongation of annealed plate gradually increases as the temperature increasing from 300 °C to 360 °C, reaching a peak in 360 °C, and then modestly decreases to 25.0% as the temperature reaching 385 °C.

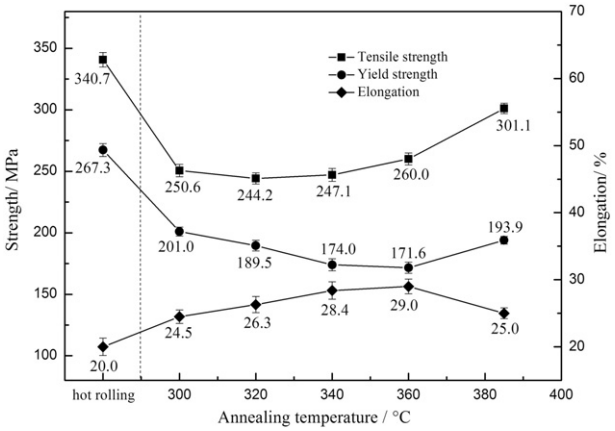

Fig. 1. Tensile property of hot rolled and annealed Al-Cu-Mg alloy plates.

Fig. 2 shows the results of fracture toughness of the rolled and annealed Al-Cu-Mg alloy plates. These values do not satisfy the criteria of plain strain and hence are conditional fracture toughness values (K_{IQ}). The K_{IQ} of hot rolled plate is more than that of annealed plates. The K_{IQ} of annealed plates has not an obvious fluctuation as the annealing temperature increases from 300 °C to 320 °C. With the temperature further increasing from 320 °C to 360 °C, the K_{IQ} slightly increases to 26.2 Mpa $*$ $m^{1/2}$. Interestingly, the K_{IQ} sharply increases to 30.9 Mpa $*$ $m^{1/2}$ as the temperature further increasing from 360 °C to 385 °C. Fig. 3 presents the fracture micrographs of plates annealed for 4 h at 340 °C and 385 °C, respectively. The fracture micrographs of two plates are characterized by large and small dimples which indicate the two annealed plates have excellent fracture toughness due to ductile fracture. There are some particles (see arrows in Fig. 3(b) and (d)) in the center of the dimples and some of them are broken. Energy spectrum analysis reveals that the atomic ratios (*Al*:*Cu*:*Mg*) of the observed

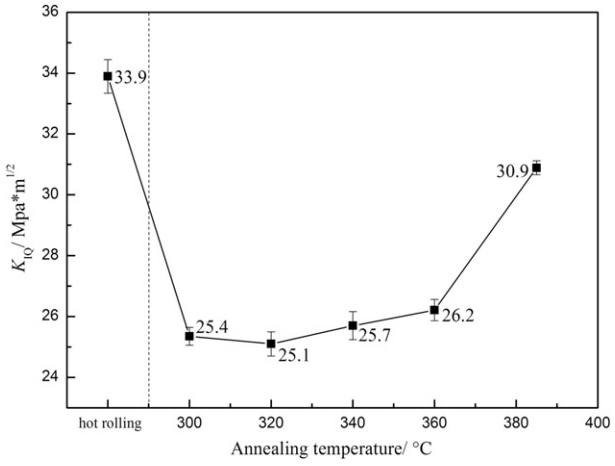

Fig. 2. Fracture toughness of Al-Cu-Mg alloy plates annealed for 4 h at different temperature.

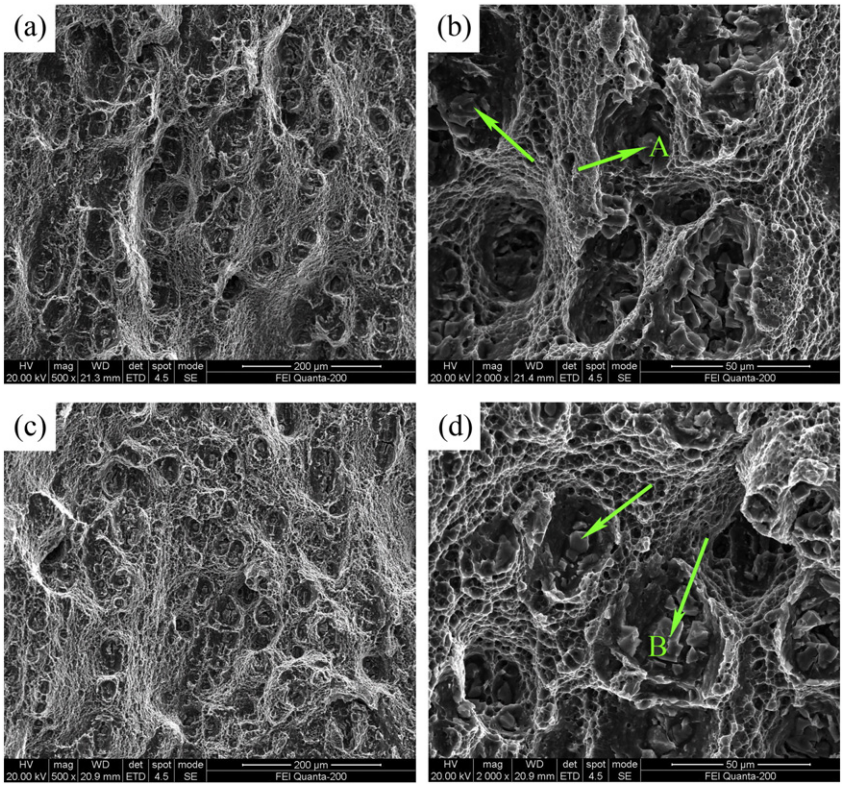

Fig. 3. Microstructure of fracture surface of Al-Cu-Mg alloy plates annealed for 4 h at 340 °C (a, b) and 385 °C (c, d).

particles (A and B) are 55.4: 22.6: 22.1 and 55.1: 21.6: 23.3, respectively. This well agrees with *S* (Al_2CuMg) phases. Those *S* (Al_2CuMg) phases may contribute to the initiation and growth of fracture crack [12,13].

Fig. 4 shows the X-ray macrotextures of the hot rolled and annealed Al-Cu-Mg alloy plates. It can be observed from Fig. 4(a) that the texture of the hot rolled Al-Cu-Mg alloy is characterized by a α-fiber texture, which runs from the Goss {011}⟨100⟩ component through the Brass orientation {011}⟨112⟩ to the P {011}⟨122⟩ component, finally to the L orientation {110}⟨011⟩ and a weak Copper {112}⟨111⟩ component. With the annealing temperature increasing from 300 °C to 385 °C, the main textures mainly fluctuate in α-fiber texture and there is no obvious intensity change for the Copper and S components. Fig. 5 presents the volume fractions of the main orientations for hot rolled and annealed plates. Brass-Goss texture, at position of (17 45 0) in Euler Space, is defined as the component between Brass and Goss in α-fiber. It can be observed from the Fig. 5 that the Brass component completely grows with the Brass-Goss component. The volume fraction of Brass component decreases firstly with the increasing temperature and then increases to the maximum value of 28.6% at 340 °C, and finally decreases again to 11.9% in 385 °C. The volume fraction of Goss component increases firstly with the increasing temperature from 300 °C to 340 °C, reaching the peak value in 340 °C, decreasing to 7.5% at 360 °C, and finally reaching the maximum value of 14.7% at 385 °C. There is no obvious fluctuation for the volume fraction of L, P, Copper and S components with the increasing temperature.

The optical micrographs microstructures of the hot rolled and the annealed Al-Cu-Mg alloy plates are shown in Fig. 6. The deformed grains in hot rolled plate are elongated parallel to the rolling direction, as shown in Fig. 6(a). When the annealing temperature is at 300 °C, some recrystallized grains occur, as indicated by an arrow in Fig. 6(b). As the temperature reaching 320 °C, the plate is partly recrystallized, with the obvious recrystallized grains (see arrows in Fig. 6(c)). There is no obvious change in microstructure of alloy plate, as annealing temperature further increasing from 320 °C to 385 °C (see Fig. 6(d–f)). Since grains are rounded/irregular in shape, based on the ASTM E112 standard, an effective grain diameter, d_c, is evaluated as

$$d_c = \sqrt{d_1 d_2} \tag{1}$$

where d_1 and d_2 are the smallest and largest grain dimensions through the geometry center of grain, respectively. The mean diameter of the grain is then given by

$$\overline{d_c} = \frac{\sum_{i=1}^{n} \sqrt{d_1 d_2}}{n} \tag{2}$$

Fig. 7 shows the distribution of grain diameter in rolled and annealed plates using OM results. To obtain reasonable statistics, at least five micrographs were used. The distribution characters of grain diameter in rolled and annealed plates all appear to be normal distribution. The average grain diameter ($\overline{d_c}$) is largest in the rolled plate. When annealing at 300 °C for 4 h, the $\overline{d_c}$ decreases to 166.5 μm. With the temperature further increasing from 300 °C to 385 °C, there is a slight downtrend in the $\overline{d_c}$ of alloy plate.

EBSD images present that the average grain size of alloy plate annealed at 385 °C for 4 h is slightly smaller than at 340 °C, as shown in Fig. 8(a) and (b). This is generally consistent with OM results. EBSD results reveal the average grain boundary misorientation of plate annealed at 340 °C for 4 h (Fig. 9(a)) is about 41.3°, and that of plate annealed at 385 °C (Fig. 9(b)) presents slight higher average boundary misorientation angle of 44.9°. Careful examinations indicate that the total number fraction of grain boundary misorientation ranged from 5° to 30° in the plate annealed at 340 °C, is obviously higher than that of plate annealed at 385 °C. Both high average boundary misorientation and small total number fraction of misorientation (from 5° to 30°), suggest the plate annealed at 385 °C is recrystallized slightly more fully than that at 340 °C, which is consistent with the fact that high annealing temperature is beneficial for recrystallization. It is observed that the cracks are easy to penetrate through most grains, which indicates the

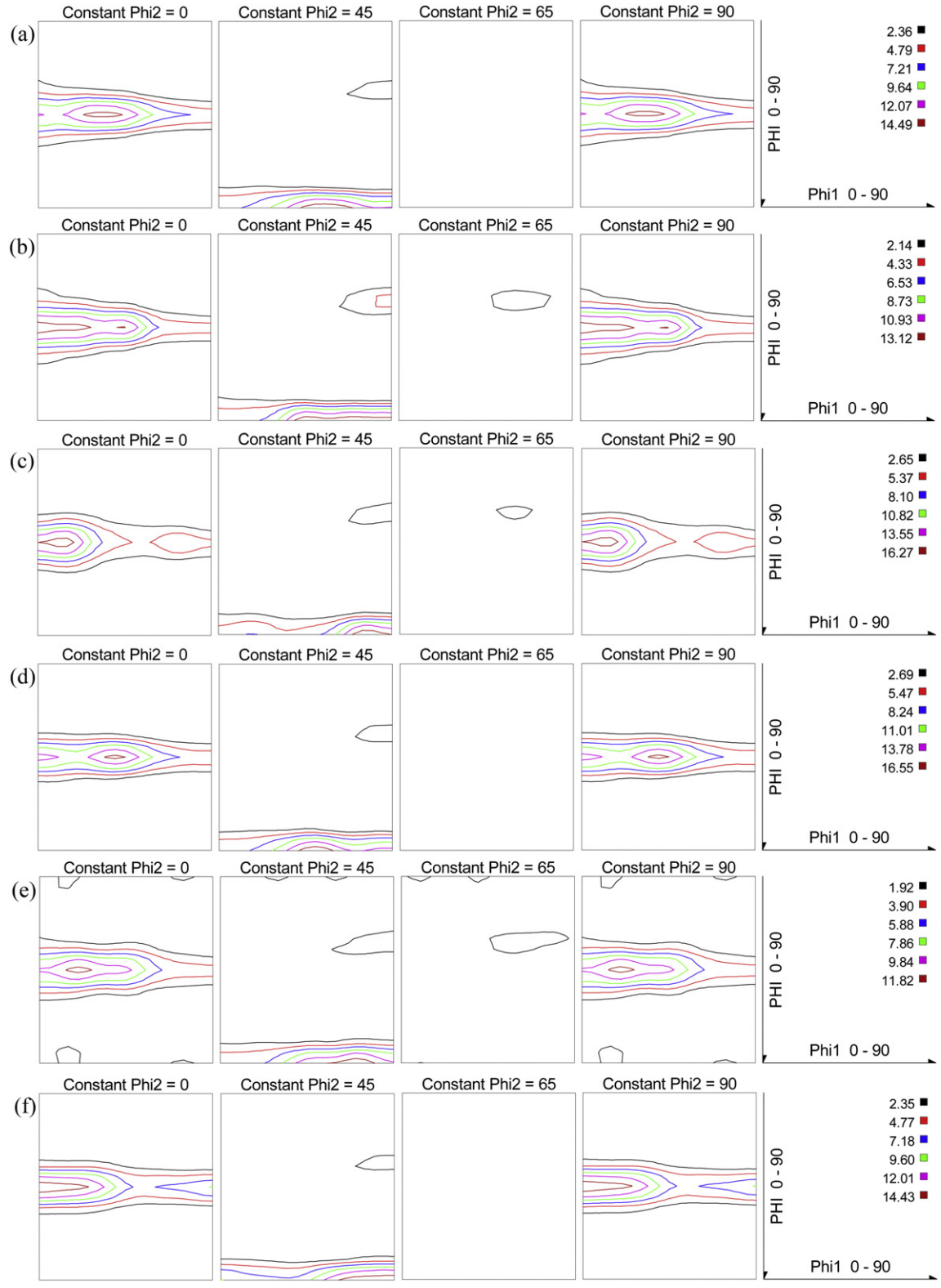

Fig. 4. ODFs representative sections of Al-Cu-Mg alloy plates hot rolled (a) and annealed for 4 h at 300 °C (b), 320 °C (c), 340 °C (d), 360 °C (e) and 385 °C (f).

failure mechanism of the two annealed plates is mainly the transgranular fracture.

4. Discussion

It is well known that annealing could decrease work hardening and benefit for the improvement of elongation in aluminum alloys. It seems abnormal that both tensile strength and yield strength sharply increase whereas elongation decreases as annealing temperature increasing from 360 °C to 385 °C. Although grain size is also one of factors that affects yield strength and elongation of alloy, the grain size of alloy plate has no obvious change, as annealing at 360 °C or 385 °C. Therefore, the different effect of grain size on tensile property could be ignored in the two plates. Obviously, the aberrant change in elongation is

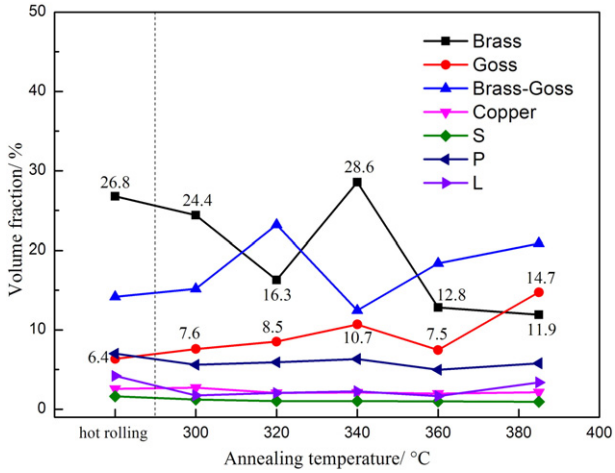

Fig. 5. Volume fractions of the main texture components in annealed Al-Cu-Mg alloy plates.

contributed by texture components. It was also reported in Ref. [5] that textures had effects on tensile property. The dominant texture components in the two annealed samples are Brass {110}⟨112⟩ and Goss {110}⟨100⟩ texture besides Brass-Goss texture. Because the effect of Brass-Goss texture on tensile property is between Brass and Goss, only Brass (110)[−112] and Goss (110)[001] are taken into consideration, respectively. As to Brass texture, the rolling plane of the plate was (110), the longitudinal direction was [−112] and the transverse direction was [1 −1 1]. In the face centered cubic metals there are 12 slip systems consisting of {111} slip planes and ⟨110⟩ slip directions. As to Goss texture, the rolling plane of the plate was (110), the longitudinal direction was [001] and the transverse direction was [−110]. On each slip plane one may calculate the Schmid factors m with respect to transverse loading directions, as listed in Table 1. In accordance with Schmid law ($\sigma_s = \tau_k / (\cos\varphi\cos\lambda)$), the critical resolved shear stress (σ_s) decreases with the increase of the m ($\cos\varphi\cos\lambda$) and no slip should occur at m = 0 [9]. Note that although the maximum Schmid factor of Goss plate is slightly more than that of Brass (indicating that Goss plate theoretically has slightly lower yield strength than that of Brass plate), the number of movable slip systems in Goss plate is 4, and only one-half that of Brass. As a consequence, the number of movable slip systems in Goss plate could play a more important role on tensile property than that of maximal m ($\cos\varphi\cos\lambda$). Therefore, the less movable slip systems in Goss plate make plasticity worse than that in Brass. As temperature increases from 360 °C to 385 °C, the elongation decreases. This is obviously due to the increasing relative volume fraction of Goss to Brass component (see Fig. 5).

It was reported that grain size had effect on fracture toughness of aluminum alloy, and smaller grain size resulted in larger grain boundary areas, therefore higher fracture toughness [14]. Fracture toughness of high strength Al-alloys is mutually influenced by yield strength and

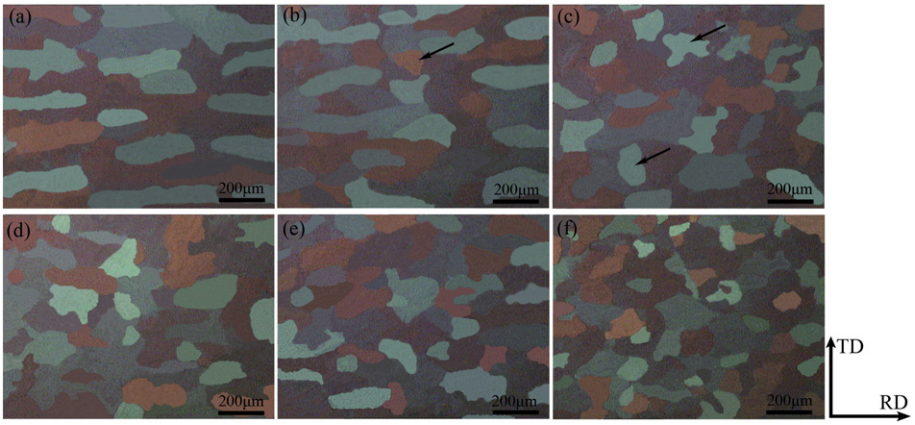

Fig. 6. Optical micrographs of the Al-Cu-Mg alloy plates hot rolled (a) and annealed for 4 h at 300 °C (b), 320 °C (c), 340 °C (d), 360 °C (e) and 385 °C (f).

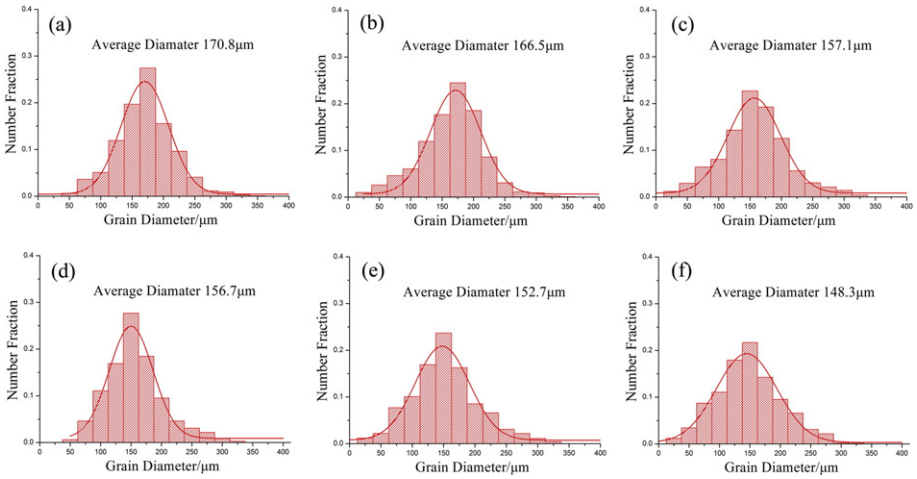

Fig. 7. OM results showing the distribution of grain diameter for Al-Cu-Mg alloy plates hot rolled (a) and annealed for 4 h at 300 °C (b), 320 °C (c), 340 °C (d), 360 °C (e) and 385 °C (f).

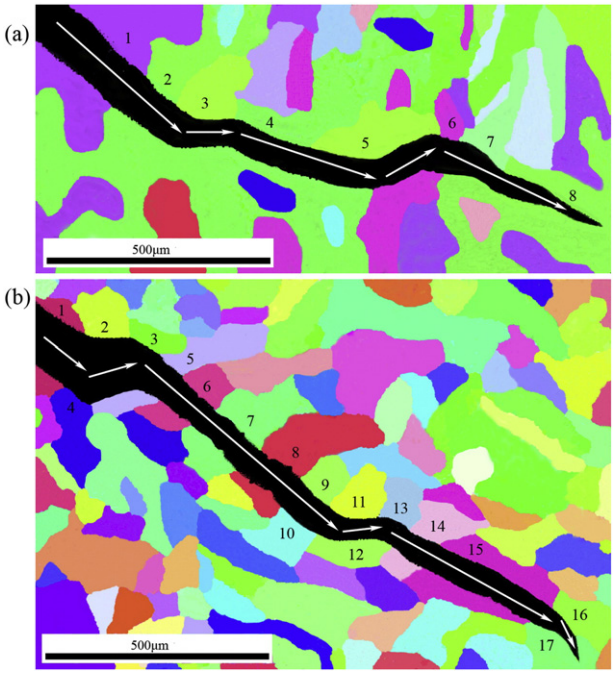

Fig. 8. EBSD results showing fracture crack propagating path for Al-Cu-Mg alloy annealed for 4 h at 340 °C (a) and 385 °C (b).

ductility, and this is particularly true as it has been reported that the requirements for high yield stress and good fracture toughness are known to be contradictory in many aluminums alloys [15–19]. Note that there is no obvious change in K_{IQ} (see Fig. 2), as annealing temperature is at 300 °C, 320 °C, 340 °C or 360 °C. When annealing at those temperatures, the $\overline{d_c}$ is fluctuant in range of 14 μm. This means that the $\overline{d_c}$ fluctuant in range of 14 μm has no obvious different effect on K_{IQ}. Comparing with the plate annealed at 360 °C, the fracture toughness of plate annealed at 385 °C is significantly higher, although the $\overline{d_c}$ difference in the two plates is only about 4 μm. Obviously, texture components have a great influence on fracture toughness. Liu et al. [8] has confirmed Goss-grains are beneficial for fatigue crack deflection, so improving the fatigue crack propagation resistance. Quietly different from the cyclic loading condition in fatigue testing, a uniaxial tensile stress, normally close to yield strength, is employed in fracture toughness testing. Under this stress condition, no crack closure effect is created during crack propagation, and the propagation rate is significantly higher than that in fatigue testing. So here is a question whether or not, Goss-grains could also contribute to fracture crack deflection under uniaxial stress condition, resulting in the improvement of fracture toughness.

As viewed from microstructure, the distinct microstructural difference between the two plates annealed at 340 °C and 385 °C respectively is the grain orientation, as shown in Figs. 4 and 8. The maximum volume fraction of Brass texture was obtained in the plate annealed at 340 °C, and the minimum volume fraction of Brass was obtained in the plate annealed at 385 °C. What's more, the volume fraction of Goss is also maximal in the plate annealing at 385 °C. This suggests the different grain orientation in the two plates is responsible for their different fracture behavior in fracture toughness testing. EBSD results reveal the fracture crack paths of the two plates are tortuous in some grains (see Fig. 8). The fracture crack in the plate annealed at 340 °C is deflected by grains 3 and 5 and that in 385 °C annealed-plate, is deflected by grains 2, 3, 11, 12, 13 and 16. In addition, little deflection occurs when cracks propagate across all the other oriented-grains in the two specimens.

Table 1
Schmid factors m of the slip system {111}⟨110⟩ for transverse loading directions in sheets containing Brass or Goss textures.

Slip plane (*hkl*)	Slip system	m (Brass)	m (Goss)
111	(111)[−110]	0.272	0
	(111)[0−11]	0.272	0
	(111)[−101]	0	0
−111	(−111)[101]	0.272	0.408
	(−111)[110]	0	0
	(−111)[0−11]	0.272	0.408
1−11	(1−11)[110]	0	0
	(1−11)[011]	0	0.408
	(1−11)[−101]	0	0.408
11−1	(11−1)[−110]	0.272	0
	(11−1)[011]	0	0
	(11−1)[101]	0.272	0

The Miller indices of grains near fracture cracks in Fig. 8(a) and (b) are presented in Table 2. The orientation of both grains 3 and 5 in the plate annealed at 340 °C, which induces crack deflection in Fig. 8(a), is close to Goss. The orientation of grain 2, grain 4 and grain 8 in Fig. 8(a) is close to Brass. Careful examination of crack path and the orientation of grains near fracture crack in Fig. 8 and Table 2, indicates the crack is remarkably deflected or obstructed when passing by Goss-oriented grains, such as grains 3 and 5 in Fig. 8(a), and grains 3, 9, 11, 12 and 16 in Fig. 8(b). In contrast, little crack deflection is detected when the cracks pass through Brass-, Copper-, S-grains and other random oriented-grains (respectively see grains 2, 4 and 8 in Fig. 8(a) and grain 7 in Fig. 8(b), grain 6 in Fig. 8(a) and grain 15 in Fig. 8(b), grain 6 in Fig. 8(b), grain 1 in Fig. 8(a), and grains 1 and 14 in Fig. 8(b)). It becomes evident that Goss-grain shows greater resistance to fracture crack propagation than other oriented-grains during fracture toughness testing.

Our previous work [8], provided a qualitative evaluation method about the twist or tilt angle component of grain boundary. In order to quantitatively evaluate the twist or tilt boundary of neighboring grains, an optimized approach is given by the present work. Schematic illustration of the orientation relationship of a grain component with its neighboring grain is shown in Fig. 10. The red crystal plane ($\boldsymbol{N_2}$) and crystal direction [$\boldsymbol{E_2}$] must be kept parallel to the green one because both of them are parallel to the EBSD specimen surface. Therefore, the red

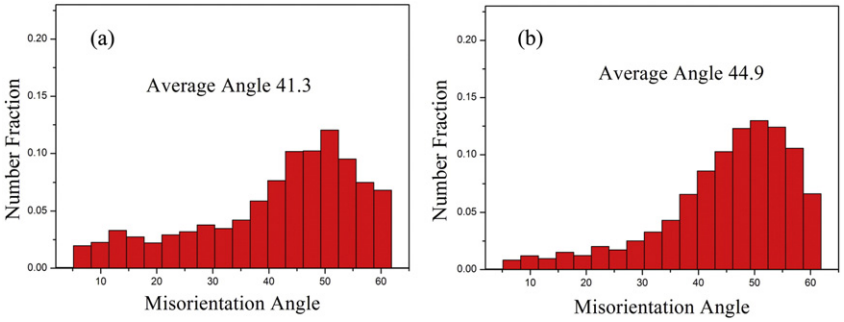

Fig. 9. EBSD results showing the grain boundary misorientation for Al-Cu-Mg alloy annealed for 4 h at 340 °C (a) and 385 °C (b).

Table 2
The grains orientation of annealed Al-Cu-Mg alloy.

Specimen	Grain	Measured indices	Simplified indices	Measured texture
Fig. 8(a)	1	(6 5 11)[11 − 11 − 1]	Close to (112)[1 − 10]	–
	2	(1 6 6)[6 − 3 2]	Close to (011)[2 − 11]	Close to Brass
	3	(1 10 12)[− 14 − 1 2]	Close to (011)[− 100]	Close to Goss
	4	(1 6 4)[2 − 1 1]	Close to (011)[2 − 11]	Close to Brass
	5	(1 10 11)[− 13 − 2 3]	Close to (011)[− 100]	Close to Goss
	6	(− 6 − 5 11)[1 1 1]	Close to (− 1 − 12)[111]	Close to Copper
	7	(9 0 10)[20 1 − 18]	Close to (101)[10 − 1]	Close to L
	8	(1 8 8)[24 − 14 11]	Close to (011)[2 − 11]	Close to Brass
Fig. 8(b)	1	(− 2 3 21)[21 7 1]	Close to (001)[310]	Close to $Cube_{ND}$
	2	(− 1 − 10 19)[11 − 3 − 1]	Close to (0 − 12)[100]	Between Goss and $Cube_{RD}$
	3	(1 12 13)[− 20 − 3 5]	Close to (011)[− 100]	Close to Goss
	4	(27 − 33 35)[19 6 − 9]	Close to (1 − 11)[62 − 3]	–
	5	(− 7 − 13 20)[29 − 11 3]	Close to (− 1 − 23)[3 − 10]	–
	6	(− 9 − 20 30)[20 9 12]	Close to (− 1 − 23)[634]	Close to S
	7	(− 1 − 18 16)[− 2 1 1]	Close to (0 − 11)[− 211]	Close to Brass
	8	(− 2 − 1 15)[11 8 2]	Close to (001)[110]	Close to H
	9	(2 11 15)[− 28 1 3]	Close to (011)[− 100]	Close to Goss
	10	(11 − 20 19)[7 1 − 3]	Close to (1 − 22)[71 − 3]	–
	11	(− 1 − 15 19)[11 − 2 − 1]	Close to (0 − 11)[100]	Close to Goss
	12	(1 12 11)[10 1 − 2]	Close to (011)[100]	Close to Goss
	13	(− 6 13 15)[19 3 5]	Close to (− 122)[100]	–
	14	(− 7 − 13 26)[13 − 7 0]	Close to (− 1 − 24)[2 − 10]	–
	15	(− 6 − 5 13)[4 3 3]	Close to (− 1 − 12)[111]	Close to Copper
	16	(− 1 − 18 23)[− 13 2 1]	Close to (0 − 11)[− 100]	Close to Goss
	17	(− 3 − 18 16)[8 − 4 − 3]	Close to (0 − 11)[2 − 1 − 1]	Close to Brass

Cube:{001}⟨100⟩; $Cube_{RD}$:{013}⟨100⟩; $Cube_{ND}$:{001}⟨310⟩; Goss:{011}⟨100⟩; Brass:{011}⟨211⟩; P:{011}⟨122⟩; L:{011}⟨011⟩; H:{001}⟨110⟩; Copper:{112}⟨111⟩; S:{123}⟨634⟩.

direction $[\boldsymbol{E_2}]$ of the grain component $(\boldsymbol{N_2})[\boldsymbol{E_2}]$, should be kept parallel with the green one of the neighboring grain$(\boldsymbol{N_1})[\boldsymbol{E_1}]$ by firstly rotating around the common tangent(CO line) of DB and OG lines, and then the rotated red crystal plane of the grain$(\boldsymbol{N_2})[\boldsymbol{E_2}]$ should also be kept parallel with the green one of the neighboring grain$(\boldsymbol{N_1})[\boldsymbol{E_1}]$ by again rotating around the rotated OG line. By this way, the grain boundary characteristic can be determined quantitatively. One can calculate the twist angle α between the two neighboring grains using this way, and the twist angle α can be expressed as:

$$\alpha = \arccos(\boldsymbol{E}_1 \cdot \boldsymbol{E}_2) \tag{3}$$

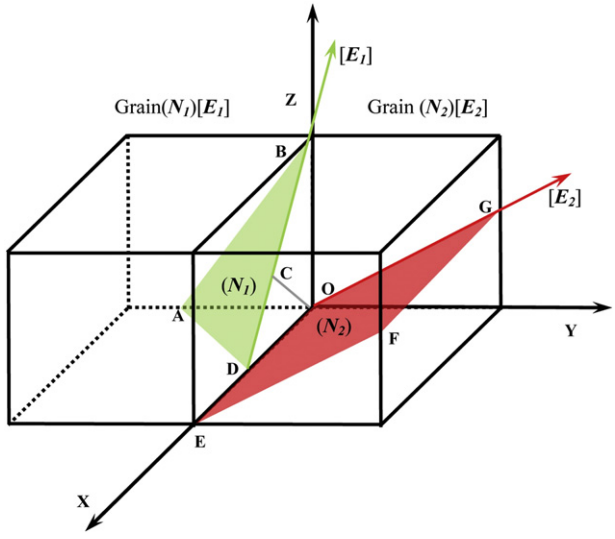

Fig. 10. Schematic illustration of the orientation relationship of the grain component $(\boldsymbol{N_1})[\boldsymbol{E_1}]$ with its neighboring grain component $(\boldsymbol{N_2})[\boldsymbol{E_2}]$.

The tilt angle β can be calculated in the following way. The unit vector of ***CO***, defined ***P***, can be expressed by the following equation:

$$\boldsymbol{P} = (\boldsymbol{E}_1 \times \boldsymbol{E}_2)/|\boldsymbol{E}_1 \cdot \boldsymbol{E}_2| \tag{4}$$

where, $|\boldsymbol{E_1} \cdot \boldsymbol{E_2}|$ is the length of $\boldsymbol{E_1} \cdot \boldsymbol{E_2}$. After rotating α angle around $\boldsymbol{P}$, $\boldsymbol{N_2}$ then converts into $\boldsymbol{N_2}'$ that can be calculated by the following equation:

$$N_{2\prime} = N_2 \cdot \cos\alpha + (\boldsymbol{P} \times \boldsymbol{N}_2)\sin\alpha + \boldsymbol{P}(\boldsymbol{P} \cdot \boldsymbol{N}_2)(1 - \cos\alpha) \tag{5}$$

So, the tilt angle β between the two neighboring grains can be described as:

$$\beta = \arccos(\boldsymbol{N}_1 \cdot \boldsymbol{N}_{2\prime}) \tag{6}$$

Table 3
The twist or tilt angles between neighboring grains in annealed Al-Cu-Mg alloy.

Specimen	Neighboring grains	α(°)	β(°)
	1 and 2	27.3	27.1
	2 and 3	140.9	11.3
	3 and 4	136.0	16.0
	4 and 5	129.5	17.9
	5 and 6	120.9	119.5
	6 and 7	86.3	75.1
Fig. 8(a)	7 and 8	70.5	59.5
	1 and 2	34.5	12.8
	2 and 3	154.9	96.5
	3 and 4	166.6	21.6
	3 and 5	145.0	18.6
	5 and 6	48.4	1.7
	6 and 7	108.1	30.3
	7 and 8	110.9	38.2
	8 and 9	139.4	39.4
	9 and 10	160.5	48.5
	9 and 11	171.7	59.3
	11 and 12	163.0	118.3
	11 and 13	152.6	15.6
	13 and 14	39.6	34.1
	14 and 15	68.9	4.4
	15 and 16	124.0	51.1
Fig. 8(b)	16 and 17	157.5	5.3

The calculated twist α and tilt β values by Eqs. (3)–(6) are presented in Table 3. It becomes evident that Goss-grains or those grains close to Goss orientation are found to have great twist angle of 136–171.7° (such as grains 2 with 3, grains 3 with 4 in Fig. 8(a), grains 9 with 11, and grains 11 with 12 in Fig. 8(b)), or great tilt angle of 75.1–119.5° with neighboring grains (see grains 5 with 6, grains 6 with 7 in Fig. 8(a), grains 2 with 3, and grains 11 with 12 in Fig. 8(b)). Remarkable crack deflections at the grain boundaries (see grains 3 and 5 in Fig. 8(a), and grains 3, 11 and 12 in Fig. 8(b)) are detected due to the great twist angle component boundary or great tilt angle component boundary. This is consistent with the reports of Zhai et al. [6,7] and Liu et al.[8] who have revealed Goss-grain has large twist or tilt boundaries with neighboring grains. Interestingly, Brass-grains or those grains close to Brass orientation are also observed to have great twist angle (108.1° and 110.9°) with S- and H– grains (see grains 6 and 7 in Fig. 8(a), and grains 7 and 8 in Fig. 8(b)), but the fracture crack is still easy to penetrate through those Brass-grains. It confirms that Goss- and Brass-grains have similar mechanism and effect on fracture toughness as it acts on fatigue performance. Great twist angle of Brass-grains with their neighboring grains don't result in obvious fracture crack deflection. This is because the direction of {111} dislocation slipping planes of Brass-grains is far away to the maximum shear stress (see {111} pole figure of Brass texture in Ref. [8]), resulting in small {111} slipping planes participating in plastic deformation in Brass-grains, stress concentration and subsequent crack damage accumulation in Brass-grains [8]. Note that S-grains are observed to have small twist (48.4°) and tilt (1.7°) angle with a neighboring random oriented grain (see grains 5 with 6 in Fig. 8(b)), and Copper-grains have relatively small twist (86.3° and 68.9°) and tilt angle (75.1° and 4.4°) with a neighboring L-grain or random oriented grain (respectively see grains 6 with 7 in Fig. 8(a), and grains 14 with 15 in Fig. 8(b)). This gives a good explanation for little fracture crack deflection observed in S- and Copper-grains.

Combined the above analyses and our previous work [8], it becomes evident that Goss-grains in the annealed Al-Cu-Mg alloy plate, having a great twist angle or tilt angle component boundary with the neighboring grains, are still able to facilitate crack deflection under the condition of uniaxial tensile stress creating no crack closure, as compared with cyclic loading condition with crack closure in fatigue testing. Goss-grains, thereby effectively retard fracture crack propagation. Brass-grains present a small resistance to crack propagation even though they have a great twist angle component boundary with neighboring grains under the uniaxial tensile stress in the toughness testing. S- and Copper-grains also show a small resistance to crack propagation due to their small twist and tilt angle component boundary with neighboring grains. Considering the continuity of texture components in α-fiber in the present work, the texture volume fraction rather than intensity, is more precise for the assessment of texture content. Obviously, the high Goss/Brass volume fraction ratio favors the improvement in fracture toughness. There is no obvious fluctuation for the volume fraction of L, P, Copper and S components in plates annealed for 4 h at different temperatures. The effect of Brass-Goss grains on fracture toughness is between Brass- and Goss-grains. It can be calculated from the Fig. 5 that the Goss/Brass ratio is about 0.31 (annealing at 300 °C), 0.52 (320 °C), 0.37 (340 °C), 0.58 (360 °C) and 1.24 (385 °C), respectively. The plate annealed at 385 °C for 4 h possesses the highest Goss/Brass ratio, which gives a good explanation for its highest fracture toughness.

5. Conclusions

The present investigation of effects of texture components on fracture toughness of annealed Al-Cu-Mg alloy plates has been performed. A new method has been proposed to accurately evaluate the twist and tilt angle of grain boundaries. The results show:

(1) Goss-grains in the annealed Al-Cu-Mg alloy, present a significant crack deflection effect similar to fatigue crack propagation, even though a uniaxial tensile stress without crack closure effect, is employed in the toughness testing.
(2) Brass-, S- and Copper-grains show little resistance to crack propagation under the uniaxial tensile stress in the toughness testing.
(3) The high Goss/Brass volume fraction ratio, is responsible for the enhanced fracture toughness in the Al-Cu-Mg alloy plate annealed at 385 °C for 4 h.

Acknowledgments

The authors are grateful for financial support from the National Key Fundamental Research Project of China (2012CB619506-3), National Natural Science Foundation of China (51171209), and 2011 Program of Ministry of Education of China.

References

[1] A.K. Vasudevan, M.A. Przystupa, W.G. Fricke Jr., Texture-microstructure effects in yield strength anisotropy of 2090 sheet alloy, Scr. Met. Mater. 24 (1990) 1429–1434.
[2] A.M. Marcus, B.L. Adams, Texture effects on yield strength in aluminum with variable grain volume distribution, Scr. Met. Mater. 27 (1992) 155–159.
[3] X.F. Wang, M.X. Guo, Y. Zhang, The dependence of microstructure, texture evolution and mechanical properties of Al-Mg-*Si*-Cu alloy sheet on final cold rolling deformation, J. Alloys Compd. 657 (2016) 906–916.
[4] Z.G. Wang, Z.F. Zhang, X.W. Li, W.P. Jia, S.X. Li, Orientation dependence of the cyclic deformation behavior and the role of grain boundaries in fatigue damage in copper crystals, Mater. Sci. Eng. A 319-321 (2001) 63–73.
[5] D.L. Chen, M.C. Chaturvedi, N. Goel, Fatigue crack growth behavior of X2095 Al–Li alloy, Int. J. Fatigue 21 (1999) 1079–1086.
[6] T. Zhai, A.J. Wilkinson, J.W. Martin, A crystallographic mechanism for fatigue crack propagation through grain boundaries, Acta meter. 48 (2000) 4917–4927.
[7] T. Zhai, X.P. Jiang, J.X. Li, M.D. Garratt, G.H. Bray, The grain boundary geometry for optimum resistance to growth of short fatigue cracks in high strength Al-alloys, Int. J. Fatigue 27 (2005) 1202–1209.
[8] Z.Y. Liu, F.D. Li, P. Xia, S. Bai, Y.X. Gu, D.E. Yu, S.M. Zeng, Mechanisms for Goss-grains induced crack deflection and enhanced fatigue crack propagation resistance in fatigue stage II of an AA2524 alloy, Mater. Sci. Eng. A 625 (2015) 271–277.
[9] F.H. Shen, D.Q. Yi, Y. Jiang, B. Wang, H.Q. Liu, C. Tang, W.B. Shou, Semi-quantitative evaluation of texture components and fatigue properties in 2524 T3 aluminum alloy sheets, Mater. Sci. Eng. A 657 (2016) 15–25.
[10] W.C. Liu, J.G. Morris, Kinetics of the formation of the β fiber rolling texture in continuous cast AA 5xxx series aluminum alloys, Scr. Mater. 47 (2002) 743–748.
[11] W.C. Liu, J.G. Morris, Comparison of the texture evolution in cold rolled DC and SC AA 5182 aluminum alloys, Mater. Sci. Eng. A 339 (2003) 183–193.
[12] M.J. Haynes, R.P. Gangloff, Elevated temperature fracture toughness of Al-Cu-Mg-Ag Sheet: characterization and modeling, Metall. Mater. Trans. A 28 (1997) 1815–1827.
[13] T.S. Srivatsan, D. Lanning Jr., Microstructure, tensile properties and fracture behavior of an Al-Cu-Mg alloy 2124, J. Mater. Sci. 28 (1993) 3205–3213.
[14] C. Qin, G.Q. Gou, X.L. Che, H. Chen, J. Chen, P. Li, W. Gao, Effect of composition on tensile properties and fracture toughness of Al–Zn–Mg alloy (A7N01S-T5) used in high speed trains, Mater. Des. 91 (2016) 278–285.
[15] V.M.J. Sharma, K. Sree Kumar, B. Nageswara Rao, S.D. Pathak, Effect of microstructure and strength on the fracture behavior of AA2219 alloy, Mater. Sci. Eng. A 502 (2009) 271–277.
[16] H.C. Fang, K.H. Chen, X. Chen, L.P. Huang, G.S. Peng, B.Y. Huang, Effect of Zr, Cr and Pr additions on microstructures and properties of ultra-high strength Al–Zn–Mg–Cu alloys, Mater. Sci. Eng. A 528 (2011) 7606–7615.
[17] Z. Zhang, K.H. Chen, H.C. Fang, X.W. Qi, G. Liu, Effect of Yb addition on strength and fracture toughness of Al-Zn-Mg-Cu-Zr aluminum alloy, Trans. Nonferrous Metals Soc. China 18 (2008) 1037–1042.
[18] N.M. Han, X.M. Zhang, S.D. Liu, B. Ke, X. Xin, Effects of pre-stretching and ageing on the strength and fracture toughness of aluminum alloy 7050, Mater. Sci. Eng. A 528 (2011) 3714–3721.
[19] D. Dumont, A. Deschamps, Y. Brechet, On the relationship between microstructure, strength and toughness in AA7050 aluminum alloy, Mater. Sci. Eng. A 356 (2003) 326–336.